Inorganic Chemistry

ARTICLE

pubs.acs.org/IC

Synthesis and Characterization of Crystalline Structures Based on Phenylboronate Ligands Bound to Alkaline Earth Cations

Marc Reinholdt,[†] Jonas Croissant,[†] Lidia Di Carlo,[†] Dominique Granier,[†] Philippe Gaveau,[†] Sylvie Bégu,[†] Jean-Marie Devoisselle,[†] P. Hubert Mutin,[†] Mark E. Smith,[‡] Christian Bonhomme,[§] Christel Gervais,[§] Arie van der Lee,[∥] and Danielle Laurencin*[,†]

[†]Institut Charles Gerhardt Montpellier ICGM, UMR 5253 CNRS-UM2-UM1-ENSCM, Pl. E. Bataillon, CC1701, 34095 Montpellier Cedex 5, France

[‡]Department of Physics, University of Warwick, CV4 7AL Coventry, United Kingdom

[§]LCMCP, UMR CNRS 7574, UPMC Université Paris 06, Collège de France, 11 place Marcelin Berthelot, 75231 Paris Cedex 05, France

[∥]Institut Européen des Membranes, CNRS - UMR 5635, Université de Montpellier 2, CC 047, Pl. E. Bataillon, 34095 Montpellier Cedex 5, France

Supporting Information

ABSTRACT: We describe the preparation of the first crystalline compounds based on arylboronate ligands $PhB(OH)_3^-$ coordinated to metal cations: $[Ca(PhB(OH)_3)_2]$, $[Sr(PhB(OH)_3)_2]\cdot H_2O$, and $[Ba(PhB(OH)_3)_2]$. The calcium and strontium structures were solved using powder and single-crystal X-ray diffraction, respectively. In both cases, the structures are composed of chains of cations connected through phenylboronate ligands, which interact one with each other to form a 2D lamellar structure. The temperature and pH conditions necessary for the formation of phase-pure compounds were investigated: changes in temperature were found to mainly affect the morphology of the crystallites, whereas strong variations in pH were found to affect the formation of pure phases. All three compounds were characterized using a wide range of analytical techniques (TGA, IR, Raman, XRD, and high resolution ^1H, ^{11}B, and ^{13}C solid-state NMR), and the different coordination modes of phenylboronate ligands were analyzed. Two different kinds of hydroxyl groups were identified in the structures: those involved in hydrogen bonds, and those that are effectively "free" and not involved in hydrogen bonds of any significant strength. To position precisely the OH protons within the structures, an NMR-crystallography approach was used: the comparison of experimental and calculated NMR parameters (determined using the Gauge Including Projector Augmented Wave method, GIPAW) allowed the most accurate positions to be identified. In the case of the calcium compound, it was found that it is the ^{43}Ca NMR data that are critical to help identify the best model of the structure.

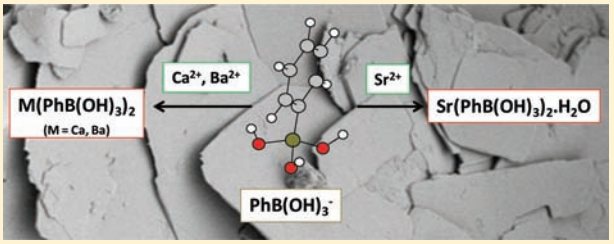

INTRODUCTION

Boronic acids ($RB(OH)_2$) form a class of compounds, which are being used in an increasing number of fields.[1] They serve as reactants for organic synthesis (notably in the Miyaura–Suzuki coupling reaction),[1,2] as sensors for the detection of anions like fluoride,[3] as enzyme inhibitors (notably in commercial drugs like Bortezomib),[1,4] as pending functional groups on stationary phases used in chromatography,[3] and also as building blocks for materials synthesis.[5]

So far, the vast majority of materials that have been prepared with boronic acid units are composed of an *organic*-only framework, and many belong to the covalent organic framework family of crystalline porous materials (COFs).[5] However, to the best of our knowledge, there has been no report of a crystalline hybrid *organic–inorganic* phase in which boronate anions $RB(OH)_3^-$ (i.e., the conjugated base of boronic acids) are used as ligands for metal cations, and the coordination chemistry of boronates has not been explored yet. Indeed, in the only crystal structure involving an arylboronate anion reported so far, the anion is not even directly bound to the metal cation Na^+.[6] Given the very wide range of applications of anionic ligands such as carboxylates, phosphonates, and sulfonates for the preparation of crystalline hybrid organic–inorganic phases like metal organic frameworks (MOFs),[7] it thus appears important to explore the coordination chemistry of boronates, because they could be used in the future as building blocks for the synthesis of new hybrid materials. Here, we report on the preparation and characterization of the first structures involving boronate ligands ($PhB(OH)_3^-$) coordinated to metal cations (Ca^{2+}, Sr^{2+}, and Ba^{2+}), and we demonstrate the structural diversity that can be obtained using these ligands. We show that by combining high resolution solid-state

Received: May 7, 2011
Published: July 14, 2011

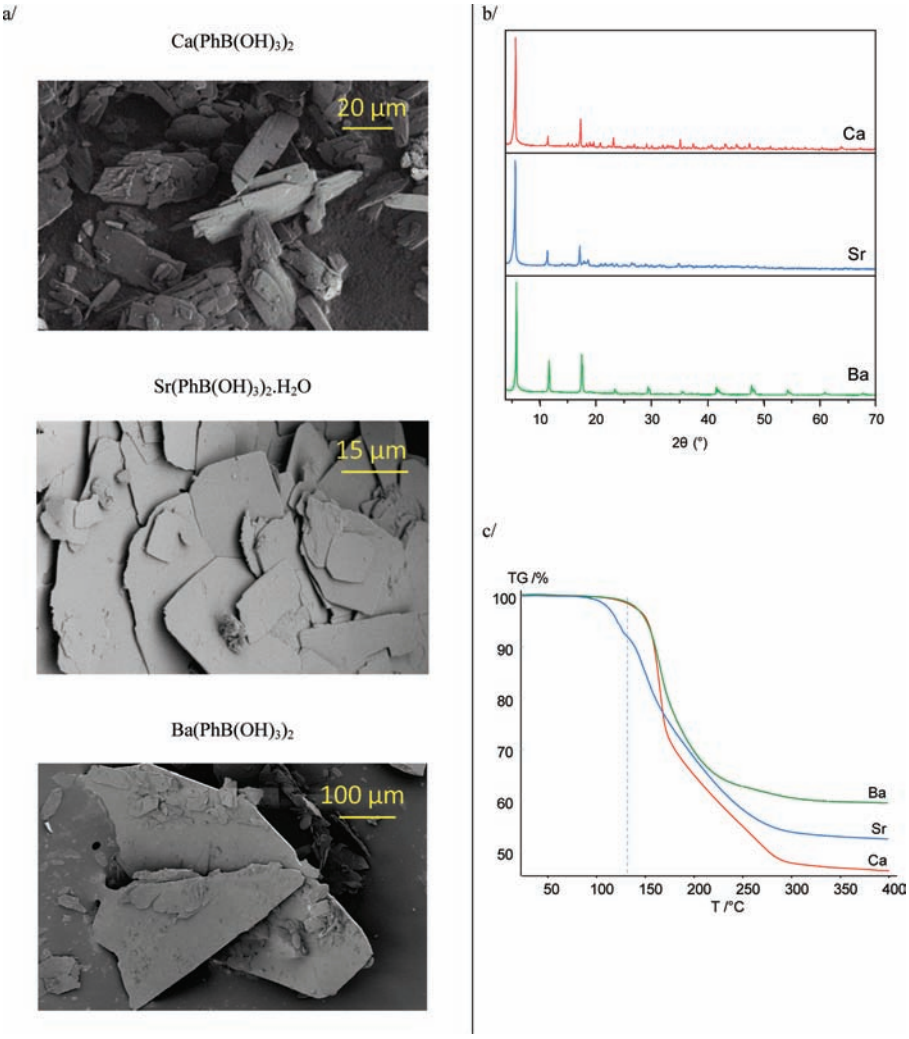

Figure 1. (a) SEM, (b) powder X-ray diffraction, and (c) TGA analyses of $Ca(PhB(OH)_3)_2$, $Sr(PhB(OH)_3)_2 \cdot H_2O$, and $Ba(PhB(OH)_3)_2$.

NMR experiments and DFT calculations, the details of the structure, and notably the H-bond networks, can be evidenced.

EXPERIMENTAL SECTION

Synthesis. Phenylboronic acid ($PhB(OH)_2$, Alfa Aesar, 98+%),[8] calcium chloride dihydrate ($CaCl_2 \cdot 2H_2O$, 99+% purity, Acros Organics), strontium chloride hexahydrate ($SrCl_2 \cdot 6H_2O$, 99+% purity, Acros Organics), barium chloride dihydrate ($BaCl_2 \cdot 2H_2O$, 99+% purity, Alfa Aesar), sodium hydroxide (NaOH, Acros Organics), and calcium carbonate ($CaCO_3$, 99+% purity, Acros Organics) were used as received. For the synthesis of the ^{43}Ca-enriched sample, ^{43}Ca-labeled $CaCO_3$ was purchased from CortecNet. All reactions were carried out using ultrapure water and absolute ethanol.

Synthesis of $Ca(PhB(OH)_3)_2$. 0.192 g (4.8 mmol, 1 equiv) of NaOH was dissolved in 14.0 mL of a 1:1 ethanol/water solution, and 0.585 g of $PhB(OH)_2$ (4.8 mmol, 1 equiv) was then added. After complete dissolution of the phenylboronic acid, the solution was heated. When the temperature reaches ~50 °C, 3.0 mL of a 0.80 mol L^{-1} aqueous solution of $CaCl_2$ (2.4 mmol, 0.5 equiv) was then added drop by drop under magnetic stirring, leading to the immediate formation of a white precipitate. The suspension was further heated to 100 °C and refluxed for 24 h. The reaction medium was then left to cool at room temperature, before being filtered under vacuum for ~15 min. The precipitate was washed twice with 10 mL of a 1:1 ethanol/water solution (with the vacuum maintained for 5 and 15 min, respectively, after each of these washings). The powder was dried by washing it twice with 10 mL of diethyl ether (with the vacuum maintained for 5 and 15 min, respectively), and then air-dried in an oven at ca. 40 °C for ~60 h. Yield: 458 mg, 60%. Several attempts to recrystallize this sample to obtain single crystals were unfortunately unsuccessful. Anal. Calcd for $C_{12}H_{16}B_2O_6Ca$: C, 45.3; H, 5.0; Ca, 12.6; B, 6.8. Found: C, 44.9; H, 5.1; Ca, 12.8; B, 6.5. Its IR and Raman spectra are given in the Supporting Information in Figure S1.

Synthesis of $Sr(PhB(OH)_3)_2 \cdot H_2O$. 0.192 g (4.8 mmol, 1 equiv) of NaOH was dissolved in 14.0 mL of a 1:1 ethanol/water solution, and 0.585 g of $PhB(OH)_2$ (4.8 mmol, 1 equiv) was then added. After complete dissolution of the phenylboronic acid, the solution was heated to 100 °C. 3.0 mL of a 0.80 mol L^{-1} aqueous solution of $SrCl_2$ (2.4 mmol, 0.5 equiv) was then added drop by drop under magnetic stirring, leading to the immediate formation of a white precipitate. The suspension was refluxed for 24 h, during which the formation of fairly large crystallites was observed. The reaction medium was then left to cool, before being filtered under vacuum for ~15 min. The microcrystalline precipitate was washed and dried as described previously for the Ca phase. Yield: 479 mg, 52%. The crystals were suitable for single-crystal X-ray diffraction. Anal. Calcd for $C_{12}H_{18}B_2O_7Sr$: C, 37.6; H, 4.7. Found: C, 37.1; H, 4.8. Its IR and Raman spectra are given in Figure S1.

dx.doi.org/10.1021/ic200961a |*Inorg. Chem.* 2011, 50, 7802–7810

Synthesis of Ba(PhB(OH)$_3$)$_2$. 0.192 g (4.8 mmol, 1 equiv) of NaOH was dissolved in 14.0 mL of a 1:1 ethanol/water solution, and 0.585 g of PhB(OH)$_2$ (4.8 mmol, 1 equiv) was then added. After complete dissolution of the phenylboronic acid, the solution was heated to 100 °C. 3.0 mL of a 0.80 mol L^{-1} aqueous solution of $BaCl_2$ (2.4 mmol, 0.5 equiv) was then added drop by drop under magnetic stirring, leading to the immediate formation of a white precipitate. The suspension was refluxed for 3 h. The warm reaction medium was then filtered. The white precipitate was washed and dried as described previously for the Ca and Sr phases and corresponded to a microcrystalline powder of Ba(PhB(OH)$_3$)$_2$ (yield: 360 mg, ∼36%). Single plate-shaped crystals of Ba(PhB(OH)$_3$)$_2$ formed in the filtrate upon cooling. However, attempts to use them to determine the crystal structure were unsuccessful (vide infra). Yield (in single crystals): 290 mg, 29%. Anal. Calcd for $C_{12}H_{16}B_2O_6Ba$: C, 34.7; H, 3.9; Ba, 33.9. Found: C, 34.7; H, 3.9; Ba, 32.5. Its IR and Raman spectra are given in Figure S1.

Synthesis of ^{43}Ca-Enriched Ca(PhB(OH)$_3$)$_2$. The ^{43}Ca-labeled Ca(PhB(OH)$_3$)$_2$ sample was prepared starting from a 3/2 mixture of 60%-labeled $CaCO_3$ and nonlabeled $CaCO_3$ (meaning that the final ^{43}Ca enrichment in the product is expected to be ∼36%). 75.8 mg of the mixture (0.75 mmol, 1 equiv) was placed in an alumina crucible and heated to 1000 °C for 3 h, to form CaO. The solid was then added to 0.575 mL of ultrapure water (contained inside a centrifuge tube), and the suspension was stirred at room temperature. 1.45 mL of a 1 mol L^{-1} solution of HCl was then added dropwise (1.45 mmol, 1.9 equiv), to form an aqueous solution of calcium chloride in the centrifuge tube. Separately, 0.061 g of NaOH (1.51 mmol, 2 equiv) was dissolved in a 2:1 mixture of ethanol and water. 0.183 g of PhB(OH)$_2$ (1.50 mmol, 2 equiv) was then added under stirring. After complete dissolution of the phenylboronic acid, this solution was added drop by drop to the $CaCl_2$ solution, leading to the immediate formation of a white precipitate. The suspension was stirred for 2 days at room temperature, then centrifuged for 30 min at 20 000 rpm. The supernatant was removed, and the white solid was suspended in 10 mL of a 1:1 water/ethanol mixture, and then centrifuged for 30 min at 20 000 rpm. After repeating once more the latter washing, a similar procedure was then used to dry the solid with 10 mL of diethylether. The white powder was finally air-dried at 80 °C for 3 days. Yield: 171 mg, 72%.

Characterization. Elemental analyses were carried out by the Service Central d'Analyse of the CNRS (Vernaison, France). IR spectra were recorded in transmission mode on KBr pellets, using an Avatar 320 FTIR spectrometer. TGA measurements were performed on a Netzsch STA 409 PC instrument. Typically about 30−45 mg of powder was heated in an alumina crucible from room temperature to 800 °C, under a flow of a nitrogen−oxygen mixture (55−60 cm^3 min^{-1}) and with a heating rate of 2 °C min^{-1}. SEM measurements were conducted on a Hitachi S4800 instrument under an excitation voltage value between 0.5 and 8 kV depending on each powder's surface charging. Powdered samples were simply deposited on double face tape and then Pt-metallized by sputtering under vacuum.

Powder X-ray Diffraction Measurements on Ca(PhB(OH)$_3$)$_2$ and Structure Resolution. Because no crystals suitable for single-crystal X-ray diffraction were found for Ca(PhB(OH)$_3$)$_2$, a structure solution from powder data was attempted. X-ray powder data were first recorded using a PANalytical X'pert MPD-Pro diffractometer at the wavelength of Cu Kα (λ = 1.5405 Å) in Bragg−Brentano scanning mode. The experimental powder pattern is shown in Figure 1 (together with those of the Sr(PhB(OH)$_3$)$_2$·H$_2$O and Ba(PhB(OH)$_3$)$_2$ phases, recorded in similar conditions). Indexing was successful using DICVOL04.[9] A triclinic unit cell was found with a figure of merit M20 of 82.5, and 54 of the 55 first peaks indexed. The volume of the unit cell, 716.53 Å^3, corresponds, with a supposed formula of $(C_6H_8BO_3)_2Ca$ with 21 non-hydrogen atoms, to a volume of 17.1 Å^3 per non-hydrogen atom, assuming *P*-1 as the space group. The structure could, however, not be solved using different specialized structure solution packages such as FOX and Topas-A.[10,11] A new measurement was done on a capillary on the SLS-MS beamline (Villigen, Switzerland), at a wavelength of λ = 0.99987 Å, and this measurement allowed the structure to be solved and refined (Figure S2).

Table 1. Crystallographic Data for Ca(PhB(OH)$_3$)$_2$ and Sr(PhB(OH)$_3$)$_2$·H$_2$O

	Ca(PhB(OH)$_3$)$_2$	Sr(PhB(OH)$_3$)$_2$·H$_2$O
CCDC	816691	816692
structure	powder	single crystal
empirical formula	$C_{12}H_{16}B_2O_6Ca$	$C_{12}H_{18}B_2O_7Sr$
M_r/g mol^{-1}	317.95	383.51
color	white powder	colorless
temperature/K	293	175
λ/Å	0.99987	0.71073
crystal system	triclinic	monoclinic
space group	*P*-1	$P2_1/c$
a/Å	5.8563(13)	6.21861(17)
b/Å	7.9937(18)	7.9567(2)
c/Å	15.6392(34)	30.7635(11)
α/deg	100.9843(12)	90
β/deg	93.4023(12)	92.783(3)
γ/deg	92.1888(13)	90
V/Å^3	716.53(27)	1520.37(8)
Z	2	4
ρ_{calcd}/g cm^{-3}	1.474	1.675
μ/mm^{-1}	0.460	3.575
$2\theta_{max}$/deg	117.381	
θ_{max}/deg		29.1
reflns collected		17 800
independent reflns		3711
obsd reflns ($I > 2\sigma(I)$)		3232
refined parameters		199
R_1 ($I > 2\sigma(I)$)		0.093
wR_2 ($I > 2\sigma(I)$)		0.066
R_1 (all data)		0.101
wR_2 (all data)		0.066
$\Delta\rho$(max/min)/e Å^{-3}		−4.30/3.70
R_p	0.03457	
wR_p	0.01162	
GOF S	1.161	0.981

The structure was solved using FOX[10] by parallel tempering on four semirigid phenyl moieties, four semirigid BO_3 groups, and one floating Ca atom. The program Topas-A[11] was then used to refine the structure using semiflexible rigid bodies for the two phenylboronate moieties. Preferential orientation was modeled using spherical harmonics; the background was modeled with Chebyshev polynomials and a $1/2\theta$ dependent function to model air scattering at low angles. One peak at ∼3.9° that is due to a kapton foil in the synchrotron beam pipe was separately modeled. The orientations and the positions of the separate rigid bodies were optimized along with the position of the Ca atom. Inside the rigid bodies a number of distances were optimized, but subject to minimum and maximum values. The torsion angles along the C−B axes were freely refined. Only isotropic atomic displacement parameters were refined, where they were constrained to be equal in each phenyl ring plus adjacent boron atom. The isotropic atomic displacement parameters of the hydrogen atoms were constrained to 1.2 times that of their parent atoms. The oxygen atoms in each BO_3 group were also

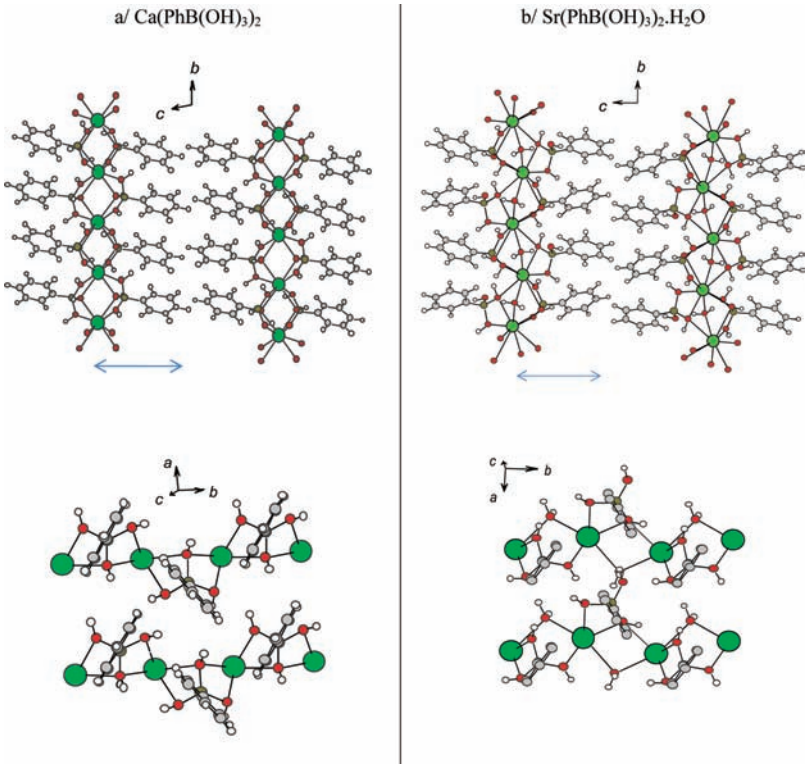

Figure 2. Representation of the crystal structures of (a) $Ca(PhB(OH)_3)_2$ and (b) $Sr(PhB(OH)_3)_2 \cdot H_2O$. M, C, H, O, and B atoms are shown in green, gray, white, red, and brown, respectively. The two figures at the bottom represent an alternate view of the part of the structure above which is indicated by a blue double arrow. In the bottom right figure, aromatic H atoms have been removed for clarity.

constrained to be equal with respect to their isotropic atomic displacement parameter. A comparison between the experimental and Rietveld refined XRD powder patterns is given in Figure S2. It is noteworthy that discrepancies remain between the experimental and calculated X-ray diffraction powder patterns, possibly because of defects in the piling of the layers along the *c* axis (as further discussed below for the Sr structure) and preferential orientation effects. Indeed, the strongest discrepancy between the experimental and refined powder XRD data is for the (00l) peaks. Attempts to refine the pattern by removing the most intense Bragg peak and including different preferential orientation modeling schemes did not lead to better results. Details on the crystallographic data can be found in Table 1.

Single-Crystal X-ray Diffraction Measurements on $Sr(PhB(OH)_3)_2 \cdot H_2O$ and Structure Resolution. A very thin platelet of the Sr compound ($0.050 \times 0.300 \times 0.350\ mm^3$) was found to be suitable for single-crystal diffraction and mounted on a Xcalibur-I four-circle diffractometer (Agilent Technologies; Mo Kα radiation, 0.71073 Å).

The crystal, and others as well, was found to be highly mosaic, which made the data reduction procedure rather delicate. The apparent mosaicity is most probably due to stacking faults of the layers, which are only held together by weak van der Waals interactions, along the *c*-axis. This becomes clear by inspection of reconstructed diffraction images of the *hnl* and *nkl* planes. Indeed, the diffraction spots of the *hk*0 diffraction planes are well distinguished and separated, whereas those of *hnl* and *nkl* display strong diffusion streaks along the *c*-axis (see Figure S3 in the Supporting Information). The structure could nevertheless easily be solved using ab initio charge flipping methods as implemented in the Superflip program.[12] All non-hydrogen atoms could be refined with anisotropic atomic displacement parameters. Hydrogen atoms could not be located in a difference map. Thus, for the phenyl moieties, they were placed geometrically, whereas for the hydroxyl groups, they were positioned using the results of DFT calculations (vide infra). The positions were then optimized with riding constraints. The program CRYSTALS was used for the structural refinements.[13] There is a relatively large residual not far from the heavy Sr atom. This is probably due to an inadequate absorption correction and/or strong mosaicity of the crystal, which causes a delicate data integration. Different absorption models were tried, as well as different data integration strategies. The best outcome is presented here. Details on the crystallographic data can be found in Table 1.

In the case of $Ba(PhB(OH)_3)_2$, despite numerous attempts to determine the structure from either single-crystal X-ray diffraction measurements or Rietveld refinements of powder patterns, no satisfactory refinement was possible yet, the *R* value being very high. This is probably due to the defects of piling along the *c* axis, the high mosaicity of the crystals (Figure S4), and the very strong preferential orientation effects observed on the XRD powder patterns (Figure 1b). Nevertheless, the different measurements performed clearly show that the barium structure is not isotypic to the other two, and a preliminary refinement was obtained.

Solid-State NMR Experiments. ^{11}B MAS NMR spectra were recorded on a Varian VNMRS 400 MHz (9.4 T) spectrometer at a frequency of 128.38 MHz, using a 3.2 mm Varian T3 HXY MAS probe. The single pulse experiments were performed with a ~45° solid pulse of 1.3 μs, a recycle delay of 6 s, and 100 kHz spinal-64 ^1H decoupling. 64 transients were recorded at a spinning speed of 20 kHz, and the chemical shifts were referenced to external $NaBH_4$ at −42.06 ppm (used as a secondary reference).

^{13}C MAS NMR spectra were recorded on a Varian VNMRS 400 MHz (9.4 T) spectrometer at a frequency of 100.62 MHz, using a 3.2 mm Varian T3 HXY MAS probe. The Cross-Polarization MAS (CPMAS) pulse sequence was used, using a contact time of 5 ms, and 100 kHz spinal-64 ^1H decoupling during acquisition. A recycle delay of 20 to 200 s was used, as ^1H relaxation was found to be very long in some of these

samples. 624 to 3584 transients were recorded at spinning speeds of 7 to 10 kHz, and the chemical shifts were referenced to external adamantane (used as a secondary reference), the high frequency peak being set to 38.5 ppm. It is noteworthy that although relative intensities of ^{13}C peaks must be carefully compared in CPMAS NMR spectra, no change in relative intensities of the ^{13}C signals was observed for the $Ba(PhB(OH)_3)_2$ phase, when increasing the contact time from 3 to 5 to 7 ms.

High resolution ^1H MAS NMR spectra were recorded on a Bruker Avance III 700 MHz (16.45 T) spectrometer at a frequency of 700.13 MHz, using a fast spinning 1.3 mm Bruker HX MAS probe. The single pulse experiments were performed with a 90° pulse of 1.8 μs and a recycle delay of 40 s. 16 transients were recorded at a spinning speed of 60 kHz, and the chemical shifts were referenced to external adamantane at 1.8 ppm from tetramethylsilane (TMS), used as a secondary reference.

The ^{43}Ca MAS NMR spectrum of ^{43}Ca-enriched $Ca(PhB(OH)_3)_2$ was recorded on a Bruker Avance III 850 MHz (19.98 T) spectrometer at a frequency of 57.22 MHz, using a 7 mm Bruker MAS probe. The single pulse experiments were performed with a 90° solid pulse of 1.5 μs and a recycle delay of 0.8 s. 1440 transients were recorded at a spinning speed of 5 kHz. Chemical shifts were referenced at 0 ppm to a 1 mol L^{-1} aqueous solution of $CaCl_2$.[14]

DFT Geometry Optimizations and NMR Calculations. Geometry optimizations based on DFT calculations were performed with the VASP (Vienna Ab-initio Simulation Package) 4.6 code[15] based on the Kohn−Sham Density Functional Theory (DFT) and using a periodic and plane-wave pseudopotential approach. Exchange-correlation was considered with the generalized gradient approximation of Perdew−Burke−Ernzerhof.[16] The integral over the first Brillouin zone was performed using a Monkhorst-Pack 2 × 2 × 2 *k*-point grid.[17] The electron−ion interaction was described by the Projector Augmented-Wave (PAW) method.[18] Energetically favorable geometries were picked with a 400 eV energy cutoff.

In the case of $Ca(PhB(OH)_3)_2$, seven different geometry optimizations were performed. For example, the geometry labeled as model 1 (M1) was obtained starting from the XRD data, and by positioning OH protons taking into account possible H-bonds, and aromatic protons by considering typical C−H distances, and then relaxing all atom positions. M2 was obtained with the same starting point as for M1, but relaxing only proton positions. Finally, M3 and M4 were obtained starting from M2 structure after modifications of proton H81 coordinates (whose calculated at a ^1H chemical shift is 0 ppm, value not observed experimentally) and relaxing then all atoms positions. The most satisfactory model (M1) is the one shown in Figure 2a, and its fractional coordinates are given in the Supporting Information (Table S1). In the case of $Sr(PhB(OH)_3)_2 \cdot H_2O$, seven different geometry optimizations were also performed following the same approach as the calcium one. The most satisfactory structure is the one shown in Figure 2b, and its fractional coordinates are given in Table S2.

The NMR parameters were calculated within Kohn−Sham DFT using the QUANTUM-ESPRESSO code[19] in which the GIPAW method[20] was implemented, keeping the atomic positions equal to the values previously calculated with VASP. The PBE (Perdew, Burke, and Ernzerhof) generalized gradient approximation[21] was used, and the valence electrons were described by norm conserving pseudopotentials[22] in the Kleinman−Bylander[23] form. The wave functions are expanded on a plane wave basis set with a kinetic energy cutoff of 1088 eV. The integral over the first Brillouin zone is performed using a Monkhorst−Pack 2 × 2 × 2 *k*-point grid. The isotropic chemical shift δ_{iso} is defined as $\delta_{iso} = -[\sigma - \sigma^{ref}]$ where σ is the isotropic shielding and σ^{ref} is the isotropic shielding of the same nucleus in a reference system as previously described.[14,24] The NMR parameters calculated for the model structures of $Sr(PhB(OH)_3)_2 \cdot H_2O$ and $Ca(PhB(OH)_3)_2$ can be found in the Supporting Information (Tables S3 and S4).

RESULTS AND DISCUSSION

Syntheses. Calcium, strontium, and barium phenylboronate phases were synthesized by precipitation at 100 °C, by addition of an aqueous solution of the cation to a solution of $PhB(OH)_3^-$. Scanning electron microscopy images of the precipitates show that they are composed of microcrystalline platelets, whose size and morphology depend on the nature of the precipitating cation (Figure 1a).

XRD powder patterns confirm the high crystallinity of the samples. In all cases, a strong peak at small angles was observed, which corresponds to an interplanar distance ∼15 Å (Figure 1b). This suggests that the compounds have a lamellar structure, by analogy with previous work on alkaline-earth phenylphosphonates.[25] From elemental analyses and TGA measurements, it appears that the formulas of the three phases are $Ca(PhB(OH)_3)_2$, $Sr(PhB(OH)_3)_2 \cdot H_2O$, and $Ba(PhB(OH)_3)_2$. Indeed, the only phase for which a weight loss is observed below ∼150 °C by TGA is the strontium one (Figure 1c), due to the loss of one water molecule.

When syntheses are carried out at room temperature, crystalline precipitates of $Ca(PhB(OH)_3)_2$, $Sr(PhB(OH)_3)_2 \cdot H_2O$, and $Ba(PhB(OH)_3)_2$ are also obtained, according to elemental analyses. However, the crystallites are smaller with a different shape, and the XRD powder patterns also slightly differ from those of the phases synthesized at 100 °C. This is best illustrated for the calcium phase. Indeed, long rods of several micrometers length form at room temperature (Figure S5), and the relative intensity of the Bragg peaks on the XRD pattern is modified (but not their positions), possibly because of preferential orientation effects. It is worth noting that the IR, Ca K-edge XANES, ^1H, and ^{13}C NMR spectra of $Ca(PhB(OH)_3)_2$ compounds prepared at room temperature are very similar to those observed when the temperature of the synthesis is higher, but that their ^{11}B NMR spectra differ (Figure S5). This suggests that the temperature of reaction only slightly affects the structure of $Ca(PhB(OH)_3)_2$ at the atomic scale and mainly around the boron.

Several synthetic conditions were varied to analyze their influence on the formation of calcium phenylboronates. First, it should be noted that by changing the water/ethanol ratio in the syntheses, or by increasing the reflux to 2 days, no significant modifications were observed. In contrast, it appears that phase pure compounds cannot be synthesized under hydrothermal conditions. Indeed, the few tests undertaken in this sense led to mixtures of phases, in which trigonal boron species could be detected by ^{11}B NMR, and with a higher fraction of calcium and boron, possibly because of the partial degradation of the boronate ligand. Furthermore, it appears that if the pH of the reaction medium is too low (below 9.5), pure $Ca(PhB(OH)_3)_2$ phases are no longer obtained. At higher pH values (∼13−14), the risk of precipitating metal hydroxides increases, and the phenylboronate ligand also appears to degrade in solution.[1]

All in all, this shows that alkaline-earth metal−boronate phases readily form in solution, provided that the pH and temperature used for the reaction are appropriate.

Description of the Crystal Structures. As expected from the powder XRD data, all three compounds have a two-dimensional organization, with planes of metal ions separated from each other by phenylboronate ligands in the interplanar space, as shown in Figure 2 for the calcium and strontium structures and in Figure S6 in the Supporting Information for the barium one.

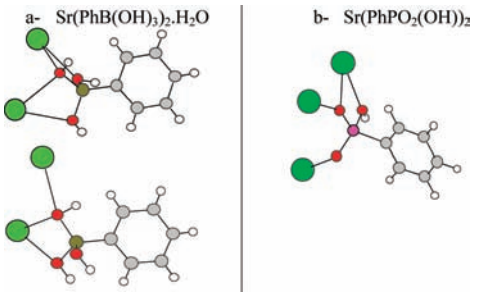

Figure 3. Comparison of the binding mode of the two inequivalent phenylboronate ligands to strontium in $Sr(PhB(OH)_3)_2 \cdot H_2O$ with the binding mode of the phenylphosphonate ligand to strontium in $Sr(PhPO_2(OH))_2$. Sr, B, P, C, H, and O atoms are represented in green, brown, pink, gray, white, and red, respectively.[26]

Concerning $Ca(PhB(OH)_3)_2$, there are two crystallographically inequivalent phenylboronate anions, which both play the role of bridging ligands (Figure 2a). Indeed, they are directly coordinated to two calcium cations through the hydroxyl groups. To be more specific, two of the three hydroxyls of the boronate are bound to one of the calcium cations, whereas the third is a μ-OH ligand bound to both cations. This results in the presence of chains of interconnected Ca^{2+} ions within the structure (Figure 2a, bottom), which interact together, leading to the planes of Ca^{2+} cations and a 2D organization of the structure. Further details on the interactions between the chains are given below.

The structure of $Sr(PhB(OH)_3)_2 \cdot H_2O$ is shown in Figure 2b. In this case, there are also two inequivalent phenylboronate ligands, which play different bridging roles. Indeed, one of the ligands has one pending OH group, which is not coordinated to any strontium cation (Figures 2b and 3a). This structure is also composed of chains of Sr^{2+} cations, in which the neighboring cations within a chain are connected through $PhB(OH)_3^-$ anions and one water molecule (Figure 2b, bottom). As for $Ca(PhB(OH)_3)_2$, these chains interact with each other to form a 2D layered structure.

The analysis of the Ca and Sr structures has evidenced different types of bridging roles for phenylboronate ligands. It is worth noting that a large variety of geometries is observed for these anions, notably because the orientation of the phenyl ring with respect to the BO_3 moiety varies from one structure to the other. Such a versatility of rotation around the B−C bond could mean that within a given structure, the phenylboronate ligand is capable of finely tuning its geometry, to reach the most stable position.

It is interesting to compare the Ca and Sr structures obtained here for phenylboronates with the lamellar structures described in the literature for phenylphosphonate ligands $PhPO_2(OH)^-$, $Ca(PhPO_2(OH))_2$ and $Sr(PhPO_2(OH))_2$.[26] Indeed, on the one hand, the phenylphosphonate structures are isotypic, which is not the case for the phenylboronate ones. On the other hand, the bridging modes observed with phenylphosphonate ligands differ from those described here with phenylboronates, as illustrated in Figure 3. Indeed, in the phosphonate structures, *three* different metal cations are connected to the oxygen atoms of the ligand. This results in the absence of a chain-like organization in the phosphonate structures, exhibiting directly a 2D layered structure, with planes of cations interconnected through phosphonate ligands.[27] Such a difference in structure within the planes is expected to lead to different properties for phosphonate and boronate families of layered materials.

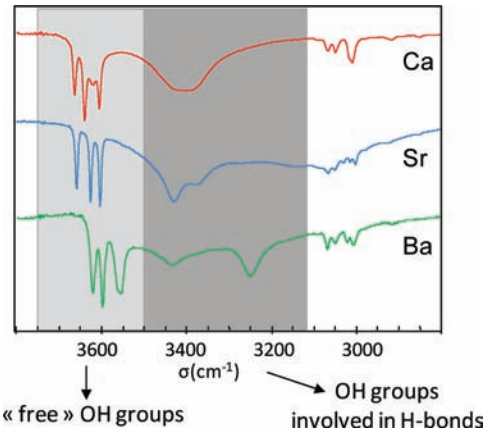

Figure 4. High frequency region of the IR spectra of $Ca(PhB(OH)_3)_2$ (red), $Sr(PhB(OH)_3)_2 \cdot H_2O$ (blue), and $Ba(PhB(OH)_3)_2$ (green).

Analysis of the Position of H Atoms. In addition to the metal−ligand bonds described above, several other interactions must exist to ensure the overall cohesion of these phenylboronate phases. First, from the Ca and Sr crystal structures, it appears that the relative orientations of the aromatic rings allow both T-shaped and parallel-displaced types of arrangements (Figure 2, bottom), which could be important for the overall stabilization of the structures. Second, hydrogen bonds between the different OH groups of the boronates must also play an important role. Indeed, IR spectroscopy confirms their presence for all compounds, as shown in Figure 4: the broad bands between 3100 and 3500 cm^{-1} correspond to OH groups involved in H-bonds, while the sharp narrow vibration bands between 3500 and 3650 cm^{-1} correspond to "free" OH groups, not involved in H-bonds. H-bonds are expected to play a particularly important role in the case of the calcium and strontium phases, by increasing the interactions between the chains of cations. Thus, to fully account for the organization of these compounds at the molecular level, it appeared important to try to determine precisely the positions of the hydrogen atoms.

Positioning hydroxyl protons within boron-containing crystal structures can be particularly challenging if they are not visible in the X-ray Fourier difference maps. Indeed, the use of neutron diffraction for boron-containing compounds is not straightforward, due to the propensity of ^{10}B to capture neutrons to form α particles and ^{7}Li.[4] Here, H atoms were positioned using DFT calculations. By looking at the O···O proximities, H atoms likely to be involved in H-bonds were first positioned, and the others were considered as "free" OH groups. The full structure was then relaxed computationally and analyzed.

Determination of the H Positions in $Ca(PhB(OH)_3)_2$. In the case of $Ca(PhB(OH)_3)_2$, several different plausible OH orientations were found. To try to determine the actual position of the hydroxyl groups within the sample, an "NMR crystallography" approach was used,[28] as solid-state NMR is a technique that is highly sensitive to atomic local environments. For each computed model, the NMR parameters of the different nuclei were calculated using the GIPAW method.[20] Results are summarized in the Supporting Information (Table S3). The expected ^{1}H, ^{13}C, ^{11}B, and ^{43}Ca solid-state NMR spectra were then simulated and

dx.doi.org/10.1021/ic200961a |*Inorg. Chem.* 2011, 50, 7802–7810

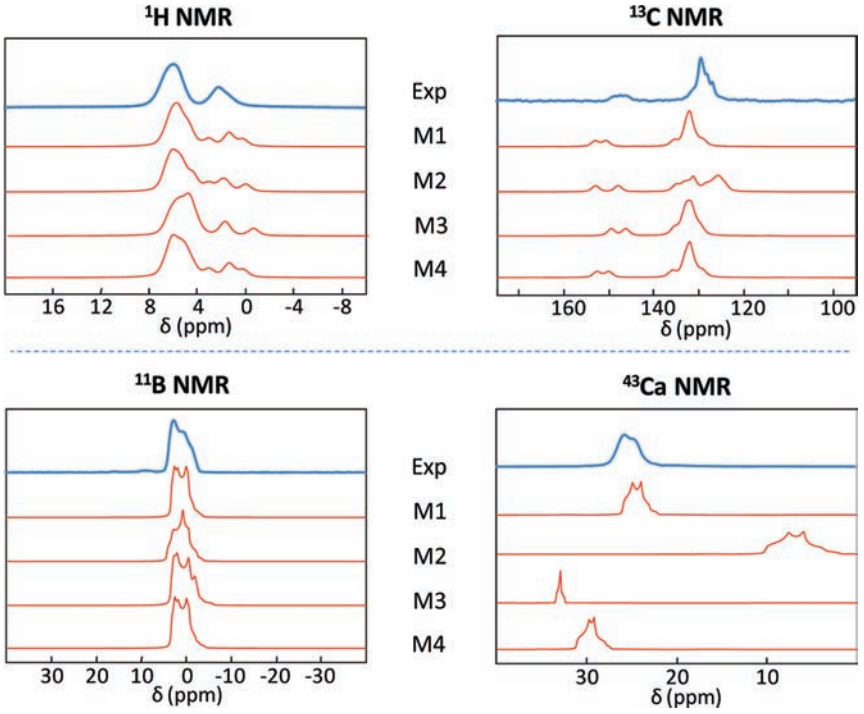

Figure 5. Experimental (blue) and calculated (red) ^{1}H, ^{11}B, ^{13}C, and ^{43}Ca solid-state NMR spectra of $Ca(PhB(OH)_3)_2$.

compared to the experimental high resolution solid-state NMR data from that sample.

The experimental MAS NMR spectra of $Ca(PhB(OH)_3)_2$ are shown in Figure 5 (in blue). In the experimental ^{1}H NMR spectrum, two broad asymmetric peaks are observed at 6.2 and 2.6 ppm, in a 3:1 ratio. The relative intensity of these signals differs from the 5:3 ratio between aromatic and hydroxyl protons in $PhB(OH)_3^-$, which suggests that some hydroxyl protons could take part in the intensity of the peak centered at 6.2 ppm. Considering previous studies related to the chemical shifts of OH groups in ^{1}H NMR,[29] the hydroxyls with the higher chemical shift are those involved in H bonds, whereas those with the lower chemical shift are the ones not involved (or less involved) in H-bonds.

On the ^{13}C NMR spectrum (recorded using a ^{1}H → ^{13}C CPMAS pulse sequence), the peaks located at ∼130 ppm correspond to the aromatic **C**−H atoms, whereas those at ∼145−152 ppm correspond to the **C**−B atoms. The ^{11}B NMR spectrum is consistent with the presence of boron in a tetrahedral environment (given the chemical shift and broadness of the signal),[30] and with two different boron local environments, in agreement with the X-ray structure. The experimental ^{11}B NMR parameters relative to each crystallographic site could be determined by recording and simulating the ^{11}B NMR spectra at two different magnetic fields (see Figure S7).

Given the very low signal sensitivity of ^{43}Ca NMR at natural abundance, a calcium phenylboronate phase enriched in calcium-43 was synthesized. It is noteworthy that in contrast with the ^{1}H, ^{11}B, and ^{13}C NMR data, the ^{43}Ca NMR data shown in Figure 5 corresponds to a sample synthesized at room temperature (and not at 100 °C). Nevertheless, as stated above, the same phase forms at both temperatures, and we also checked using Ca K-edge XANES that the Ca local environment of a sample synthesized at room temperature is the same as for one prepared at 100 °C (see Figure S5). In the experimental ^{43}Ca NMR spectrum, a second order quadrupolar line shape characteristic of a single Ca local environment is observed,[30] in agreement with the X-ray data.

The NMR spectra calculated for 4 DFT-relaxed models of $Ca(PhB(OH)_3)_2$ are shown in Figure 5 (in red). None of the models gives a perfect reproduction of the experimental data. In particular, it should be noted that there is systematically a small shift between experimental and calculated ^{13}C NMR data. This could be due to a problem of referencing of the calculated ^{13}C chemical shifts for this compound, as similar effects have been observed when dealing with a new family of compounds.[31] Nevertheless, for one of these models (M2), the calculated NMR parameters are all very different from the experimental ones (especially the ^{43}Ca NMR data), suggesting that the hydroxyl positions are inaccurate in this case. For the three other models (M1, M3, and M4), the calculated ^{1}H, ^{13}C, and ^{11}B NMR spectra are fairly similar, making it difficult to decide which is the most appropriate model. However, only the calculated ^{43}Ca NMR spectrum of M1 agrees with the experimental one, meaning that the M1 structure corresponds to the most accurate model of $Ca(PhB(OH)_3)_2$. Indeed, in the other models, the ^{43}Ca chemical shift and/or line shape clearly disagree with the experiment. A careful look at the local environment of calcium in the M1 to M4 models shows that the average Ca···O bond distance differs from one model to the other (Table S5), and this is directly reflected on the ^{43}Ca NMR spectra, because ^{43}Ca NMR chemical shifts have been shown to be very sensitive to the average Ca···O bond distance.[14,32] All in all, this work underscores the importance of recording experimental spectra of challenging nuclei like calcium-43, because the most challenging nuclei can often provide the clearest evidence for determining in detail the structure of complex compounds.

By examining the structure of model M1, it appears that some H atoms of the hydroxyls are clearly engaged in interchain

OH···O hydrogen bonds. Indeed, for two OH···O configurations, the following average geometric characteristics are observed: (O)H···O distances ∼1.8 Å, O(H)···O distances ∼2.78 Å, and (OHO) angles ∼164°. According to the classification proposed by Jeffrey, this means that they correspond to "moderate" H-bonds.[33] It is worth noting that the calculated ^{1}H chemical shifts for the corresponding hydroxyl protons are 5.6 and 5.8 ppm, and that among the six inequivalent OH groups, they are the only ones with chemical shifts in the range of those of the aromatic C−**H** protons. This explains the 3:1 relative intensity of the two broad signals observed on the ^{1}H NMR spectra, as it corresponds to the (10 + 2):4 ratio expected from the NMR calculations.

Determination of the H Positions in Sr(PhB(OH)$_3$)$_2$·H$_2$O. The experimental ^{1}H, ^{13}C, and ^{11}B NMR spectra of Sr(PhB(OH)$_3$)$_2$·H$_2$O are shown in Figure S8, together with the calculated NMR spectrum of the most satisfactory DFT model. The calculated NMR parameters are given in Table S4. Two main peaks are observed by ^{1}H NMR, with a ratio of ∼3:1. The appearance of the ^{1}H NMR spectrum is at first surprising, because it is similar to the one recorded for Ca(PhB(OH)$_3$)$_2$, despite the fact that both structures are very different, notably because of the water molecule in the strontium phase.

Finding reasonable positions for the hydroxyl protons was not straightforward for this phase, notably because in some of the models the (O)H···Sr distances were found to be very short (<2.5 Å). In the "best" DFT model, the shortest (O)H···Sr distance is ∼2.74 Å, which is reasonable considering previous work on strontium structures like SrHPO$_3$·H$_2$O.[34] A close examination of the H-bond network reveals the presence of four interchain OH···O bonds (Figure S9), the two strongest being those involving the water ligand. A close examination of the calculated ^{1}H chemical shifts shows that the water protons have shifts of 7.3 and 7.8 ppm, and that one of the other protons involved in the H bonds has a shift of 5.0 ppm, which means that they are part of the broad high frequency ^{1}H NMR signal, which can explain the aspect of the ^{1}H NMR spectrum.

All in all, using an NMR crystallography approach, it was possible to propose proton positions for both Ca(PhB(OH)$_3$)$_2$ and Sr(PhB(OH)$_3$)$_2$·H$_2$O, and thus show that there are several H bonds between the chains of cations, which participate in the stabilization of the 2D-planes.[35] However, it should be noted that despite the presence of these interactions, which lead to an overall lamellar organization, no intercalation properties could yet be evidenced for these two phases: attempts to intercalate molecules such as butanol or pyrene have so far been unsuccessful.

CONCLUSION

This article describes the first crystal structures involving RB(OH)$_3^-$ ligands directly coordinated to metal cations. Three different architectures were obtained by simply varying the nature of the alkaline earth metal (Ca, Sr, or Ba). Phenylboronate ligands were found to play a bridging role between different metal cations and to present different modes of binding. The versatility of their coordination modes and geometries within these structures was underscored. H-bonding was found to play an important role in the crystallization and organization of these phases in the solid state. For the calcium and strontium structures, it was possible to gain insight into the arrangement of the hydroxyl groups and H-bonds within the structures by using the combination of XRD, multinuclear high resolution solid-state NMR, and DFT calculations. The importance of recording the solid-state NMR spectra of the metal cations to determine the exact structure of such organic−inorganic materials was clearly demonstrated by the ^{43}Ca NMR data of Ca(PhB(OH)$_3$)$_2$, thereby suggesting that it would be worth recording ^{87}Sr and $^{135/137}$Ba NMR spectra of the other two phases, which is another challenge in itself given the NMR characteristics of these isotopes.[36]

The Ca(PhB(OH)$_3$)$_2$ and Sr(PhB(OH)$_3$)$_2$·H$_2$O phases were found to be composed of 1D chains, which interact through H-bonds to form layers, whereas preliminary results on the barium structure suggest that a 2D organization can be directly obtained. Thus, it appears that by carefully selecting the metal cation or boronate ligands, it should be possible to prepare crystalline phases with a 2D layered structure using these anions, and further studies are being carried out in this direction in our group. More generally, such structures should open up interesting perspectives for materials science, given the wide range of applications of layered materials, and it may even be possible to prepare boronate phases with a 3D organization, as is the case for MOFs, by using ligands with several boronate functions.

ASSOCIATED CONTENT

Supporting Information. Figure S1: IR and Raman spectra of Ca(PhB(OH)$_3$)$_2$, Sr(PhB(OH)$_3$)$_2$·H$_2$O, and Ba(PhB(OH)$_3$)$_2$. Figure S2: Rietveld plot for the refinement of the structure of Ca(PhB(OH)$_3$)$_2$. Figure S3: Selection of reconstructed diffraction images for Sr(PhB(OH)$_3$)$_2$·H$_2$O. Figure S4: Selection of reconstructed diffraction images for Ba(PhB(OH)$_3$)$_2$. Figure S5: Comparison of the SEM, XRD, ^{11}B NMR, and Ca K-edge XANES data of Ca(PhB(OH)$_3$)$_2$ phases prepared at room temperature or under reflux. Figure S6: Structural representation of Ba(PhB(OH)$_3$)$_2$, resulting from preliminary refinement tests. Figure S7: Experimental ^{11}B MAS NMR spectra of Ca(PhB(OH)$_3$)$_2$ recorded at 9.4 and 14.1 T, and their simulation. Figure S8: Experimental and calculated ^{1}H, ^{13}C, and ^{11}B MAS NMR spectra of Sr(PhB(OH)$_3$)$_2$·H$_2$O and Ba(PhB(OH)$_3$)$_2$. Figure S9: Representation of the interchain H bonds in Sr(PhB(OH)$_3$)$_2$·H$_2$O. Figure S10: 2D ^{1}H−^{1}H NOESY NMR spectrum of Ba(PhB(OH)$_3$)$_2$. Table S1: Fractional coordinates of the atoms of Ca(PhB(OH)$_3$)$_2$ after relaxation of all atomic positions (model M1). Table S2: Fractional coordinates of the atoms of Sr(PhB(OH)$_3$)$_2$·H$_2$O after relaxation of all atomic positions. Table S3: ^{1}H, ^{11}B, ^{13}C, and ^{43}Ca calculated NMR parameters for various models of Ca(PhB(OH)$_3$)$_2$. Table S4: ^{1}H, ^{11}B, and ^{13}C calculated NMR parameters for the best model of Sr(PhB(OH)$_3$)$_2$·H$_2$O. Table S5: Comparison of the calculated ^{43}Ca NMR parameters and the average Ca···O bond distance in the models of Ca(PhB(OH)$_3$)$_2$. This material is available free of charge via the Internet at http://pubs.acs.org. The experimental cif files corresponding to the Ca(PhB(OH)$_3$)$_2$ and Sr(PhB(OH)$_3$)$_2$·H$_2$O crystal structures have been deposited by the Cambridge Crystallographic Data Centre (No. CCDC-816691 and 816692).

AUTHOR INFORMATION

Corresponding Author

*Fax: +33 4 6714 3852. E-mail: dlaurenc@univ-montp2.fr.

■ ACKNOWLEDGMENT

This work was supported by the 7th European framework program (Marie Curie ERG 239206) and a Royal Society partnership grant (JP090313). Synchrotron X-ray experiments were conducted at the SLS-MS beamline, PSI Villigen (Switzerland), and we thank A. Cervellino for the measurements. DFT calculations were performed on the IDRIS supercomputer centre of the CNRS (Project 091461). The UK 850 MHz solid-state NMR Facility used here was funded by EPSRC, BBSRC, and the University of Warwick, and also partly funded through the Birmingham Science City Advanced Materials Project supported by AWM and the European Regional Development Fund. We acknowledge the French synchrotron SOLEIL for provision of synchrotron radiation facilities (project 20090572), and D. Vantelon for her help with the measurements. D. Bourgogne and D. Cot are acknowledged for their help in the Raman and SEM characterizations.

■ REFERENCES

(1) Hall, D. G. *Boronic Acids: Preparation, Applications in Organic Synthesis and Medecine*; Wiley-VCH: Weinheim, 2005.

(2) Miyaura, N.; Suzuki, A. *Chem. Rev.* **1995**, *95*, 2457.

(3) Nishiyabu, R.; Kubo, Y.; James, T. D.; Fossey, J. S. *Chem. Commun.* **2011**, *47*, 1106.

(4) Yang, W.; Gao, X.; Wang, B. *Med. Res. Rev.* **2003**, *23*, 346.

(5) (a) Nishiyabu, R.; Kubo, Y.; James, T. D.; Fossey, J. S. *Chem. Commun.* **2011**, *47*, 1124. (b) Severin, K. *Dalton Trans.* **2009**, 5254. (c) El-Kaderi, H. M.; Hunt, J. R.; Mendoza-Cortés, J. L.; Côté, A. P.; Taylor, R. E.; O'Keeffe, M.; Yaghi, O. M. *Science* **2007**, *316*, 268.

(6) Cammidge, A. N.; Goddard, V. H. M.; Gopee, H.; Harrison, N. L.; Hughes, D. L.; Schubert, C. J.; Sutton, B. M.; Watts, G. L.; Whitehead, A. J. *Org. Lett.* **2006**, *8*, 4071.

(7) (a) Férey, G. *Chem. Soc. Rev.* **2008**, *37*, 191. (b) Long, J. R.; Yaghi, O. M. *Chem. Soc. Rev.* **2009**, *38*, 1213. (c) Shimizu, G. K. H.; Vaidhyanathan, R.; Taylor, J. M. *Chem. Soc. Rev.* **2009**, *38*, 1430. (d) Zhao, D.; Timmons, D. J.; Yuan, D.; Zhou, H.-C. *Acc. Chem. Res.* **2011**, *44*, 123. (e) Maniam, P.; Näther, C.; Stock, N. *Eur. J. Inorg. Chem.* **2010**, 3866. (f) Plabst, M.; Bein, T. *Inorg. Chem.* **2009**, *48*, 4331. (g) Gándara, F.; García-Cortés, A.; Cascales, C.; Gómez-Lor, B.; Gutiérrez-Puebla, E.; Iglesias, M.; Monge, A.; Snejko, N. *Inorg. Chem.* **2007**, *46*, 3475.

(8) It should be noted that the purity of the phenylboronic acid precursors must be verified. Indeed, in some cases, the sample purchased turned out to be $(PhBO)_3$, whereas in others, traces of $B(OH)_3$ were present (as shown by ^{11}B solution NMR by the presence of an extra small peak at ~19.3 ppm). Recrystallization of the phenylboronic acid is recommended prior to synthesis.

(9) Boultif, A.; Louër, D. *J. Appl. Crystallogr.* **2004**, *37*, 724.

(10) Favre-Nicolin, V.; Cerny, R. *J. Appl. Crystallogr.* **2002**, *35*, 734.

(11) *TOPAS-Academic V3 by Coelho Software*; Brisbane, Australia, July, 2005.

(12) Palatinus, L.; Chapuis, G. *J. Appl. Crystallogr.* **2007**, *40*, 786.

(13) Betteridge, P. W.; Carruthers, J. R.; Cooper, R. I.; Prout, K.; Watkin, D. J. *J. Appl. Crystallogr.* **2003**, *36*, 1487.

(14) Gervais, C.; Laurencin, D.; Wong, A.; Pourpoint, F.; Woodward, B.; Howes, A. P.; Pike, K. J.; Dupree, R.; Mauri, F.; Bonhomme, C.; Smith, M. E. *Chem. Phys. Lett.* **2008**, *464*, 42.

(15) Kresse, G.; Hafner, J. *Phys. Rev. B* **1994**, *49*, 14251.

(16) (a) Perdew, J. P.; Burke, K.; Ernzerhof, M. *Phys. Rev. Lett.* **1996**, *77*, 3865. (b) Zhang, Y.; Yang, W. *Phys. Rev. Lett.* **1998**, *80*, 890.

(17) Monkhorst, H. J.; Pack, J. D. *Phys. Rev. B* **1976**, *13*, 5188.

(18) Blöchl, P. E.; Jepsen, O.; Andersen, O. K. *Phys. Rev. B* **1994**, *49*, 16223.

(19) Giannozzi, P.; Baroni, S.; Bonini, N.; Calandra, M.; Car, R.; Cavazzoni, C.; Ceresoli, D.; Chiarotti, G. L.; Cococcioni, M.; Dabo, I.; Dal Corso, A.; de Gironcoli, S.; Fabris, S.; Fratesi, G.; Gebauer, R.; Gerstmann, U.; Gougoussis, C.; Kokalj, A.; Lazzeri, M.; Martin-Samos, L.; Marzari, N.; Mauri, F.; Mazzarello, R.; Paolini, S.; Pasquarello, A.; Paulatto, L.; Sbraccia, C.; Scandolo, S.; Sclauzero, G.; Seitsonen, A. P.; Smogunov, A.; Umari, P.; Wentzcovitch, R. M. *J. Phys.: Condens. Matter* **2009**, *21*, 395502.

(20) Pickard, C. J.; Mauri, F. *Phys. Rev. B* **2001**, *63*, 245101.

(21) Perdew, J. P.; Burke, K.; Ernzerhof, M. *Phys. Rev. Lett.* **1997**, *78*, 1396.

(22) Troullier, N.; Martins, J. L. *Phys. Rev. B* **1991**, *43*, 1993.

(23) Kleinman, L.; Bylander, D. M. *Phys. Rev. Lett.* **1982**, *48*, 1425.

(24) Gervais, C.; Profeta, M.; Lafond, V.; Bonhomme, C.; Azaïs, T.; Mutin, H.; Pickard, C. J.; Mauri, F.; Babonneau, F. *Magn. Reson. Chem.* **2004**, *42*, 445.

(25) (a) Lima, C. B. A.; Airoldi, C. *Solid State Sci.* **2002**, *4*, 1321. (b) Zima, V.; Svoboda, J.; Benes, L.; Melanova, K.; Trchova, M. *Solid State Sci.* **2006**, *8*, 1380.

(26) Stone, J. W.; Smith, M. D.; zur Loye, H.-C. *J. Chem. Crystallogr.* **2007**, *37*, 103.

(27) The preliminary structure obtained for $Ba(PhB(OH)_3)_2$ (Figure S6) suggests that in this phase, one of the phenylboronate ligands is coordinated to three different barium cations. For this compound, the overall connectivity between barium and phenylboronate ligands leads directly to a two-dimensional organization of the inorganic layer.

(28) (a) Harris, R. K.; Wasylishen, R. E.; Duer, M. J. *NMR Crystallography, Encyclopedia of Magnetic Resonance*; Wiley: New York, 2009. (b) Harris, R. K.; Cadars, S.; Emsley, L.; Yates, J. R.; Pickard, C. J.; Jetti, R. K. R.; Griesser, U. J. *Phys. Chem. Chem. Phys.* **2007**, *9*, 360. (c) Salager, E.; Day, G. M.; Stein, R. S.; Pickard, C. J.; Elena, B.; Emsley, L. *J. Am. Chem. Soc.* **2010**, *132*, 2564.

(29) Pourpoint, F.; Gervais, C.; Bonhomme-Coury, L.; Azaïs, T.; Coelho, C.; Babonneau, F.; Mauri, F.; Alonso, B.; Bonhomme, C. *Appl. Magn. Reson.* **2007**, *32*, 435.

(30) (a) MacKenzie, K. J. D.; Smith, M. E. *Multinuclear Solid State NMR of Inorganic Materials*; Pergamon Materials Series, Pergamon Press: Elmsford, NY, 2002. (b) Smith, M. E.; van Eck, E. R. H. *Prog. Nucl. Magn. Reson. Spectrosc.* **1999**, *34*, 159.

(31) Johnston, J. C.; Iuliucci, R. J.; Facelli, J. C.; Fitzgerald, G.; Mueller, K. T. *J. Chem. Phys.* **2009**, *131*, 144503.

(32) Bryce, D. L. *Dalton Trans.* **2010**, *39*, 8593.

(33) (a) Jeffrey, G. A. *An Introduction to Hydrogen Bonding*; Oxford University Press: Oxford, 1997. (b) Steiner, T. *Angew. Chem., Int. Ed.* **2002**, *41*, 48.

(34) Mahmoudkhani, A. H.; Langer, V. *Phosphorus, Sulfur Silicon Relat. Elem.* **2001**, *176*, 83.

(35) In the case of the barium phase, high-resolution ^1H NMR spectra have also been recorded (Figure S8), as well as a 2D $^1H-^1H$ NOESY NMR spectrum (Figure S10), to gain insight into the hydroxyl proton positions. However, for this compound, no fully satisfying structural model was yet found.

(36) (a) Sustrino, A.; Lu, C.; Lipson, R. H.; Huang, Y. *J. Phys. Chem. C* **2009**, *113*, 21196. (b) Bowers, G. M.; Lipton, A. S.; Mueller, K. T. *Solid State NMR* **2006**, *29*, 95. (c) Hamaed, H.; Ye, E.; Udachin, K.; Schurko, R. W. *J. Phys. Chem. B* **2010**, *114*, 6014.